AGU PUBLICATIONS

JGR

Journal of Geophysical Research: Atmospheres

RESEARCH ARTICLE
10.1002/2016JD025063

Key Points:
- Improved method of horizontal averaging for better comparability of flux data in heterogeneous environments presented
- Comparison of urban CO_2 mole fraction to regional background records
- Long-term (10 years) trends and variability of urban CO_2 flux and mole fraction reported

Correspondence to:
M. Schmutz,
mi.schmutz@unibas.ch

Citation:
Schmutz, M., R. Vogt, C. Feigenwinter, and E. Parlow (2016), Ten years of eddy covariance measurements in Basel, Switzerland: Seasonal and interannual variabilities of urban CO_2 mole fraction and flux, *J. Geophys. Res. Atmos.*, *121*, 8649–8667, doi:10.1002/2016JD025063.

Received 9 MAR 2016
Accepted 27 JUN 2016
Accepted article online 2 JUL 2016
Published online 19 JUL 2016

Ten years of eddy covariance measurements in Basel, Switzerland: Seasonal and interannual variabilities of urban CO_2 mole fraction and flux

M. Schmutz[1], R. Vogt[1], C. Feigenwinter[1], and E. Parlow[1]

[1]Research Group Meteorology, Climatology, and Remote Sensing, University of Basel, Basel, Switzerland

Abstract Eddy covariance (EC) measurements of carbon dioxide (CO_2) in urban environments are carried out widely since the late nineties. However, long-term time series are still rare and little is known about long-term tendencies, even though cities are major sources of CO_2 globally. Here a full decade of EC measurements from Basel, Switzerland, is presented. An approach for the calculation of horizontal averages is presented. It improves the significance and comparability of measured fluxes from heterogeneous environments and emphasizes the need of adequate weighting by horizontal averaging in such heterogeneous urban environments, especially for the derivation of cumulative quantities like the annual net ecosystem exchange. The urban CO_2 mole fraction (ρ_C) is compared with regional background measurements, and good agreement in terms of long-term trend and seasonal variability is found. Over the last decade an increase of 2 ppm y^{-1} is observed, both locally and globally. CO_2 flux (F_C) data are analyzed for diurnal and seasonal cycles as well as interannual variabilities. F_C shows a large interannual variability in times of high source activity (e.g., during the day and in winter). In contrast, a relatively constant background flux of 5 μmol m^{-2} s^{-1} is found during periods of low source activity. The long-term trend of F_C is mostly superimposed by the large temporal variability and is found to be −5% over the last 10 years.

1. Introduction

1.1. Importance of Long-Term CO_2 Records

Recently, many studies focused on approaches toward a better understanding of the linkage between carbon dioxide (CO_2) emissions in urban environments and their controlling factors [*Christen et al.*, 2011; *Contini et al.*, 2012; *Lietzke et al.*, 2015; *Velasco et al.*, 2014]. Modeling approaches are an important step forward to transform information from point measurement to larger spatial (e.g., city) scales, which is essential to achieve a comprehensive picture of the entire urban metabolism.

The significance and resilience of the results, however, depend strongly on whether the emission factors and theoretical assumptions can be validated by reliable measurement-based data sets. As the eddy covariance (EC) method for the determination of turbulent fluxes of mass and energy only became a widely applicable method in urban areas since the late nineties, multiyear studies able to catch long-term trends and interannual variabilities are still rare. A comprehensive overview of recent studies on urban CO_2 fluxes (F_C) is given in *Lietzke et al.* [2015], whereas the longest time series reported in literature cover at most 5–6 years [*Crawford et al.*, 2011, *Gioli et al.*, 2012]. In contrast, there are numerous long-term data sets of CO_2 mole fraction (ρ_C) and F_C from natural terrestrial ecosystems (e.g., FLUXNET, www.fluxdata.org) or remote background concentration measurements (e.g., Carbon Dioxide Information Analysis Center, http://cdiac.ornl.gov/) and a variety of corresponding studies [*Hofmann et al.*, 2009; *Liu et al.*, 2015]. Taking into account, that urban areas are responsible for large parts of the global greenhouse gas emissions (~50%, depends on methodology and boundary definition of urban areas [*Intergovernmental Panel on Climate Change* (*IPCC*), 2014; *Marcotullio et al.*, 2013]), still little is known about one of the major sources of atmospheric CO_2 [*Rosenzweig et al.*, 2010].

Compared to most natural ecosystems, urban areas are hot spots of changes and development, and thus, it is barely possible to characterize and understand the ongoing processes by looking at a "short-term" snapshot of the current state. Relationships between emissions and their drivers derived from single years are not implicitly valid for longer time periods, and the validity of reported correlations still needs to be proved. Because urban CO_2 is subject to cycles on daily, weekly, and yearly scales, it is inevitable that multiple years are needed in order to detect trends and periods on all relevant time scales.

1.2. Measuring Urban Carbon Dioxide

Research on the complex pathways of CO_2 in the urban landscape is a substantial contribution to the rapid progress in urban climatology over recent years. Whereas tracking of, e.g., fuel consumption or use of other commodities linked to greenhouse gas emissions can be achieved on national or regional scales by inventory approaches, the task becomes increasingly more sophisticated for the densely populated urban environment. Major sources of CO_2 in cities are well known, most being linked to the massive energy demand of the urban metabolism (flows of material and energy caused by human activity). Large parts of urban CO_2 is caused by fuel combustion for heating, transportation, industry, and power generation and to a minor degree by processes like waste decomposition or human respiration [*Christen*, 2014]. Effective sinks of CO_2, e.g., vegetation are rare and cover only minor, patchy fractions of cities. Therefore, urban environments are normally net sources of CO_2 all over the year [*Christen et al.*, 2011; *Crawford et al.*, 2011; *Lietzke and Vogt*, 2013]. The need of adequate monitoring systems to quantify the impact of cities to the total CO_2 budget is obvious, and a large number of studies about measurement and modeling of urban air pollution have been released during the last decade. Current research on local-scale urban micrometeorology focuses on the link between direct measurements of CO_2 and its controlling factors derived from geographic information system (GIS) data (e.g., land use, traffic count, and local climate zones) [*Lietzke et al.*, 2015] or on bottom up modeling of emission processes tuned by experimental data [*Christen et al.*, 2011].

A comprehensive overview on measurement techniques to quantify greenhouse gas emissions from cities is given in *Christen* [2014], who discusses different approaches for mesoscale, local-scale, and microscale data acquisition. Regardless of theoretical and technical challenges, the EC technique provides probably the best way to determine local-scale urban CO_2 emissions from a point measurement. If the measurements take place within the urban inertial sublayer (ISL), the footprint extends several hundred meters upwind and the measured flux represents a well-mixed CO_2 signal from the corresponding area. The application of a sectorial analysis allows attributing the flux data to distinct sources or land use classes within the footprint area. Many studies have shown that, e.g., correlations can be found between F_C and traffic volume or heating activity indices [*Helfter et al.*, 2011; *Lietzke and Vogt*, 2013; *Lietzke et al.*, 2015; *Pataki et al.*, 2009; *Pawlak et al.*, 2011; *Velasco et al.*, 2005]. Despite the theoretical requirements [*Aubinet et al.*, 2012] of the EC-method (e.g., horizontal homogeneity and stationarity) are barely satisfied, EC measurements turned out to deliver reliable results even for the heterogeneous urban environment if an appropriate station setup is chosen as suggested by *Feigenwinter et al.* [2012].

The aim of this study is to contribute to an enhanced understanding of the seasonal and interannual variabilities of ρ_C and F_C by analysis of 10 years of EC data from an urban area in Basel, Switzerland, between 2005 and 2014.

2. Material and Methods

2.1. Study Site

Long-term urban meteorological measurements are carried out by the University of Basel, MCR-Lab (Meteorology, Climatology, and Remote Sensing) in the city of Basel. An 18 m tall tower is mounted on the flat roof top of the 20 m high MCR building (BKLI, 47.56173°N, 7.58049°E) since 2003. The neighborhood of the site is mainly characterized by the inner ring street Klingelbergstrasse to the east with heavy traffic, oriented along the 200°/20° axis, as well as by residential buildings enclosing green backyards, to the west. Furthermore, some tall university buildings are located approximately 250 m to the north and the northeast of the site. An aerial image of the surrounding is given in Figure 1, specific land use characteristics are depicted in Figure 2, and a summary of land use classes per sector can be found in Table 1. The site characteristics are described in more detail in *Lietzke and Vogt* [2013], where a second tower has been operated in an adjacent street canyon from mid-October 2009 until end of March 2011.

2.2. Measurements and Data Processing

The EC system of the BKLI site is operative since May 2004, and thus covering now more than a decade of measurements. The instruments are mounted to a vertical extension at the tower top at a total height of 39 m above street level (Figure 3). According to *Lietzke and Vogt* [2013] and *Feigenwinter et al.* [2012], the measurements take place above the roughness sublayer, but inside the ISL. The EC system consists of an

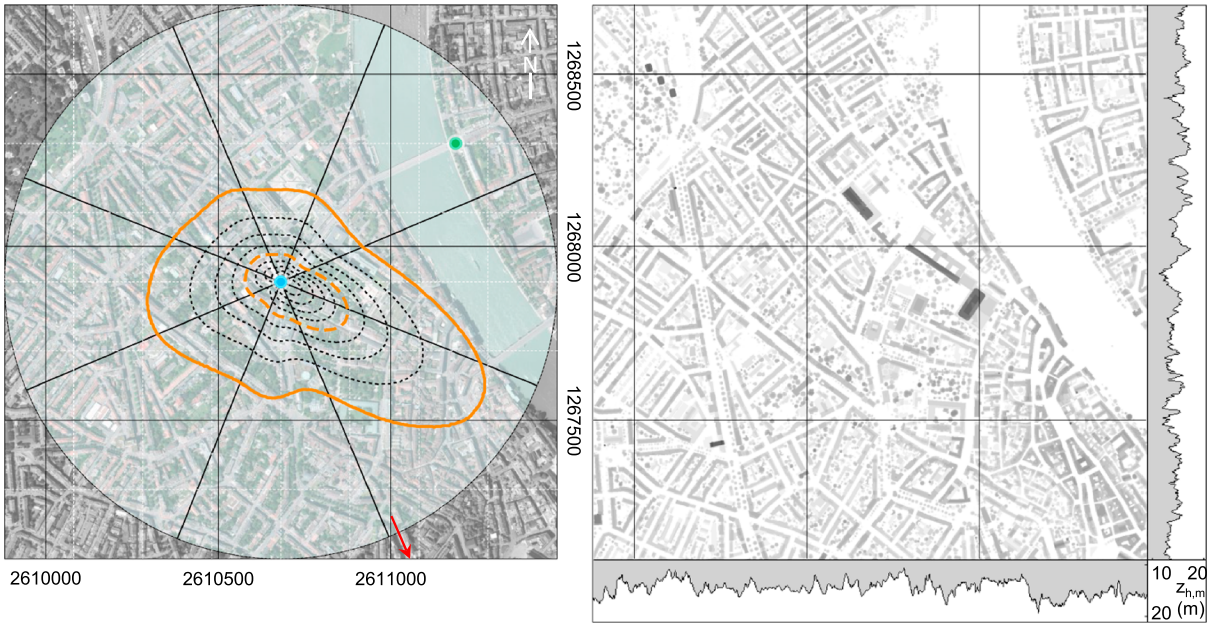

Figure 1. On the left site an aerial image (1.6 km × 1.6 km) [*Geodaten Kanton Basel-Stadt*, 2015] centered around the BKLI site (2610678/1267902, blue dot) is shown. Traffic counts at Johanniterbrücke (BJH, green dot) and Heuwaage (BHA, not on map, red arrow) are marked. The white dashed grid lines indicate steps of 200 m from the measurement site, whereas the black grid represents the Swiss coordinate system (LV03, EPSG:21781). Additionally, the average footprint estimation is shown. The thick solid and dashed orange lines indicate the 90% and 50% contour, respectively. The thin dashed black lines give additional information on the contour shape in steps of 10%. The radial black lines indicate sectors of 45° used during this study. On the right site the corresponding digital elevation data of the surrounding is shown. Building height is scaled white (0 m) to black (62.4 m). Profiles on the right and at the bottom of the graph present the median building height.

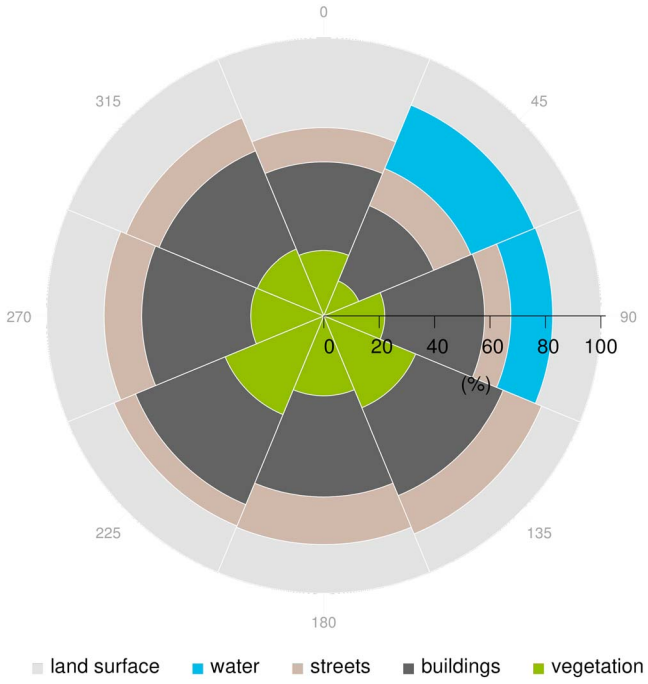

Figure 2. Fractions of land surface, water, roads, buildings, and vegetation per sector within a radius of 500 m around the BKLI site. Sectors are as defined in Figure 1, and details are listed in Table 1.

ultrasonic anemometer (=sonic, HS-50, Gill Instruments Ltd.) and an open path CO_2/H_2O infrared gas analyzer (=IRGA, LI-7500, LI-COR Inc.), both facing northward, allowing the predominant winds from east and west to pass the measuring volume mostly undisturbed. Sensor separation is 0.4 m, and the gas analyzer is tilted 35° in order to reduce the influence of water droplets on the windows. Both, the sonic and the IRGA are sampled at 20.83 Hz, whereas the IRGA is connected to the analogue input of the sonic. Thus, the internal quality control value (Automatic Gain Control) of the IRGA is not available. To calibrate the IRGA N_2 (dry) is used as zero gas and N_2/CO_2 (500 ppm) for the span.

Raw data are stored as 30 min files of orthogonal wind components u, v, and w; acoustic temperature T_s; as well as the voltage signals of the IRGA, which were converted into concentrations and later into mole fractions of CO_2 and H_2O during postprocessing

Table 1. Sectorial and Average Characteristics of the BKLI Site[a]

	z_0 (m)	z_h (m)	λ_i(%)	λ_w(%)	λ_s(%)	λ_b(%)	λ_v(%)
337.5°–22.5°	5.7	18.8	32.2	0.0	12.4	32.0	23.5
22.5°–67.5°	8.5	18.1	17.8	24.8	14.5	29.3	13.7
67.5°–112.5°	4.0	19.0	17.4	15.1	9.5	36.0	22.0
112.5°–157.5°	3.2	15.3	14.9	0.0	15.0	34.2	35.9
157.5°–202.5°	4.7	14.7	17.6	0.0	17.2	36.4	28.8
202.5°–247.5°	5.4	16.1	18.1	0.0	8.4	35.0	38.5
247.5°–292.5°	3.5	15.4	20.7	0.0	13.6	39.3	26.4
292.5°–337.5°	2.5	16.0	22.8	0.0	12.9	38.3	26.0
Mean	3.8	16.7	20.2	5.0	12.9	35.1	26.9

[a]Land use fractions λ_i (land surface), λ_w (water), λ_s (streets), λ_b (buildings), and λ_v (vegetation) are calculated for 500 m radius around the measurement site. Roughness length z_0 is derived from logarithmic wind profile during neutral conditions, and z_h is calculated from a 3-D city model.

(0–5 V = 10–30 mmol m^{-3}). The sonic is operated in uncalibrated mode, and a matrix correction [*Vogt*, 1995] was applied afterward. Average 30 min statistics were calculated using EddyPro® v5.2.1 (LI-COR Inc.). During processing, axis rotation for tilt correction, linear detrending, covariance maximization, as well as the Webb-Pearman-Leuning terms for compensation of density fluctuations [*Webb et al.*, 1980] were applied. Furthermore, data were corrected for high-pass and low-pass filtering effects [*Moncrieff et al.*, 1997, 2005], and statistical tests for raw data screening following *Vickers and Mahrt* [1997] were used. For quality check flags were calculated from steady state and developed turbulent conditions tests [*Foken et al.*, 2005; *Foken and Wichura*, 1996; *Göckede et al.*, 2007].

To avoid streamline distortion from the sonic spars and the IRGA, the wind sector 180° ± 15° was generally rejected and treated with special care during gap-filling later on. In addition to the above data removal criteria, data are rejected during rain events ±2 h and during maintenance activities. Overall data availability after completion of postprocessing is approximately 70% for flux data and up to 98% for other meteorological quantities.

2.3. Gap-Filling Algorithm

Data loss due to postprocessing, maintenance, and system failures is up to 30% for flux data. Among the different approaches for gap-filling discussed in literature [*Falge et al.*, 2001; *Moffat et al.*, 2007; *Schmidt et al.*,

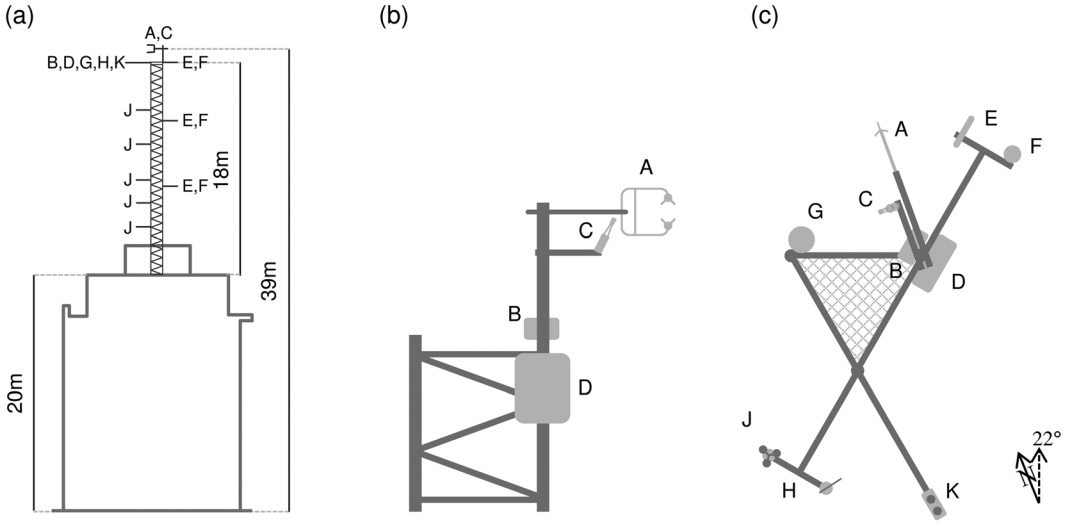

A: Gill HS-50 Ultrasonic Anemometer, **B:** Sonic Electronics Box, **C:** LI-7500 CO_2/H_2O Analyzer Sensor Head, **D:** LI-7500 Control Box, **E:** Aspirated Thermocouple, **F:** HMP155 Humidity and Temperature Probe, **G:** THYGAN Thermohygrometer, **H:** WA15 Crossarm, **J:** WAA151 Cup Anemometer, **K:** CNR1 Net Radiometer

Figure 3. (a) Side view of institute building and flux tower, (b) close-up view of EC setup at tower top, and (c) layout of complete instrumentation at tower-top level. Drawings are not to scale and aligned along the buildings orientation toward 22°.

2008], the most common methods are artificial neural networks, nonlinear regression analysis, or look-up tables (LUTs). For this study an improved moving LUT (mLUT) technique [*Reichstein et al.*, 2005] is implemented. Instead of LUTs based on static bins for specific temporal and meteorological conditions, the gap-filling values are derived from a temporal moving frame. These moving frames for a gap at a certain day, time, and wind direction (d_G, t_G, and α_G) are defined as $d_G \pm 45$ days, $t_G \pm 1.5$ h, and $\alpha_G \pm 22.5°$. Compared to the static LUT technique, the mLUT algorithm has the disadvantage of a much smaller sample size, because only few neighboring values meet the criteria. At the same time, the mLUT technique benefits from a better representativeness of the gap-filled values for a specific point in time because only temporally adjacent data are considered. This is not the case, if, e.g., data from multiple years are used for the calculation of static LUT. Due to the usage of static LUT, statistics of the time series tend to converge toward the LUT, whereas mLUTs preserve the temporal variability on a much smaller temporal scale. This is crucial, if interannual variability or long-term trends are investigated. Data availability after application of the gap-filling algorithm is at least 98%.

2.4. Horizontal Averaging

CO_2 fluxes measured by the EC method always represent an integrated signal from all sources and sinks within the footprint area. At BKLI, the sources and sinks are not evenly distributed around the station, and thus, the footprint composition and the resulting flux clearly vary with wind direction. In addition, the frequency of occurrence of wind directions changes with daytime and season; thus, there is no equilibrium between data sampled during, e.g., daytime and nighttime or in different seasons. The values measured at the tower are thus only valid for this specific point in space with the corresponding wind system and do not represent the general properties of the surrounding area. Therefore, it is necessary to consider horizontal averages in order to achieve fluxes representative for a certain spatial scale (e.g., neighborhood scale).

The basic concept of horizontal averaging goes back to *Raupach and Shaw* [1982], and different applications of horizontal averages are described by *Rotach* [1993], *Rotach* [1995], or *Christen* [2005], who showed the benefit for comparison of simultaneous measurements at different locations. In order to consider the uneven sampling of different scenarios (daytime/nighttime, weekday/weekend, seasons, and wind sectors) an adapted concept of horizontal averaging has been implemented following *Lietzke et al.* [2015], who introduced a method for the calculation of so-called "expected fluxes." Instead of weighting sectorial fluxes by the relative frequency of occurrence of the corresponding wind direction, for each sector (s) a gap-filled (X, only values from this sector) time series $F_{CX}(s)$ is generated. Subsequently, the arithmetic average is calculated out of the sectorial values for each point in time (t) which leads to the horizontal average

$$< F_C >= \frac{1}{8} \sum_{s=1}^{8} F_{CX}(s,t).$$

All terms in angle brackets in the current study are calculated following the above method.

2.5. Long-Term Development of the Urban Neighborhood

Long-term measurements of F_C are not only affected by the diurnal and seasonal variations of the local sources and sinks but also by changes in footprint composition which are caused by modifications of the city structure or variations of the urban metabolism. Modification of the land use structure like new buildings/streets, political decisions (e.g., new traffic concepts), or generally population growth is influencing the local source/sink regime and has to be taken into account when interpreting the results.

From analysis of GIS data [*Geodaten Kanton Basel-Stadt*, 2015], information about the development of the surrounding building structure could be derived. In general, there was only little construction activity during the last 10 years. An exception is the newly built (2007–2010) "Universitäts-Kinderspital" (Children's Hospital) 200 m north-northeast, which replaces a former hospital building of similar shape. Furthermore, demolition work has begun in summer 2014 in the backyard to the west of the institute, and there is ongoing construction work for the new "Biozentrum" (Center for Molecular Life Sciences) 300 m to the north since 2013.

For the Klingelbergstrasse information about traffic volume is available from a permanent traffic count 500 m northeast, at the Johanniterbrücke (BJH) and approximately 1.3 km to the other direction at the Heuwaage (BHA) for the entire measurement period, both on an hourly resolution [*Geodaten Kanton Basel-Stadt*, 2015]. Between 2004 and 2007 the average daily traffic volume at BJH was approximately 20,000 veh day^{-1}.

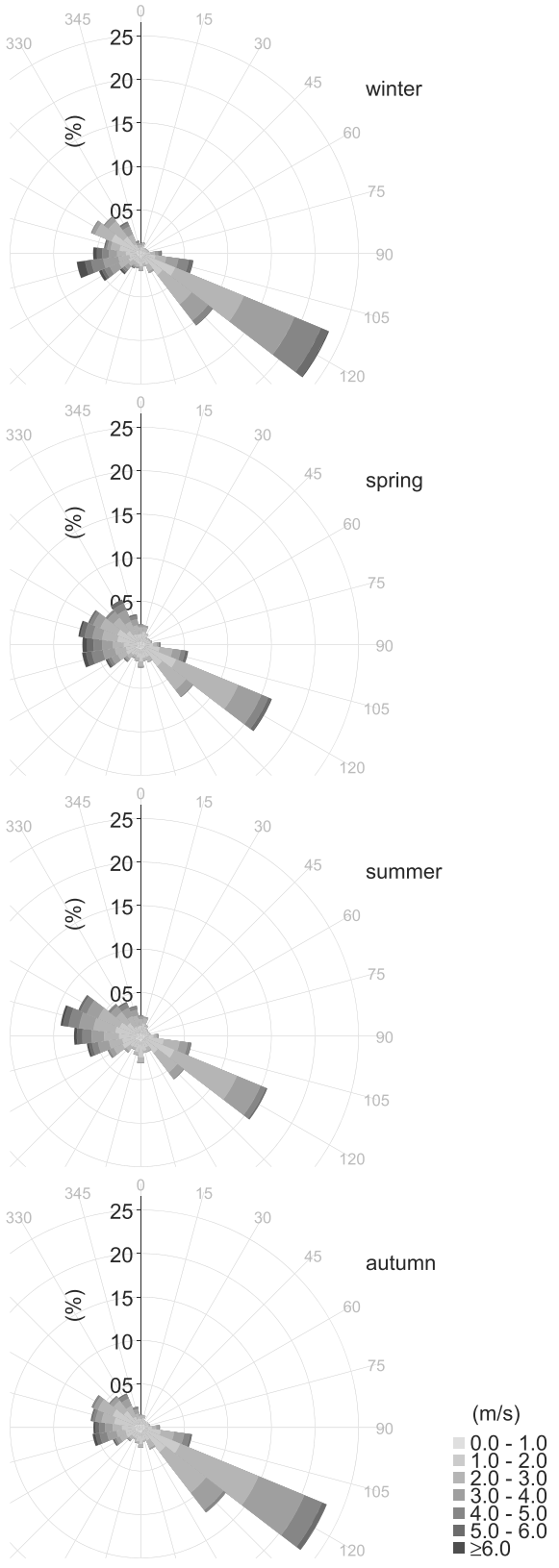

Figure 4. Seasonal relative frequencies of wind direction and velocity at BKLI (24 bins based on 30 min averages).

With the opening of the traffic bypass "Nordtangente" in 2007/2008 the average daily number of vehicles has steadily diminished to roughly 15,000 veh day^{-1} until 2011 and then stayed more or less constant.

In 2013 the local authorities reported a total population of 173,330 inhabitants for the city of Basel (without agglomeration). The total population growth since 2004 is 3.9%, whereas the yearly growth rate is 0.43% for the whole city and varies between 0.24 and 0.65% for the residential districts around BKLI [*Statistisches Amt Basel-Stadt*, 2015].

2.6. Definition of Wind Sectors and Seasons

For the application of sectorial analysis, data were separated into eight wind sectors of equal width (45°) (Figure 1 and Table 1). Sectors are numbered clockwise from 1 to 8 starting at north. For the analysis of seasonality the four seasons winter (December-January-February), spring (March-April-May), summer (June-July-August), and autumn (September-October-November) are distinguished following the meteorological convention. Thus, if yearly values are indicated, December is always attributed to the following year.

3. Results and Discussion

3.1. Meteorology at the BKLI Site

The climate of Basel is characterized by mild winters and warm summers (Cfb-climate according to Köppen classification). The yearly temperature amplitude calculated from monthly averages is 18 K, whereas minima and maxima can be around 0°C and 25°C, respectively. Average rainfall is 804 mm and is distributed all over the year with a maximum during summer. In Figure 4 the average seasonal wind roses for the 10 years show the dominant wind directions ESE and W/NW. The local wind system has a distinct diurnal cycle, where ESE and

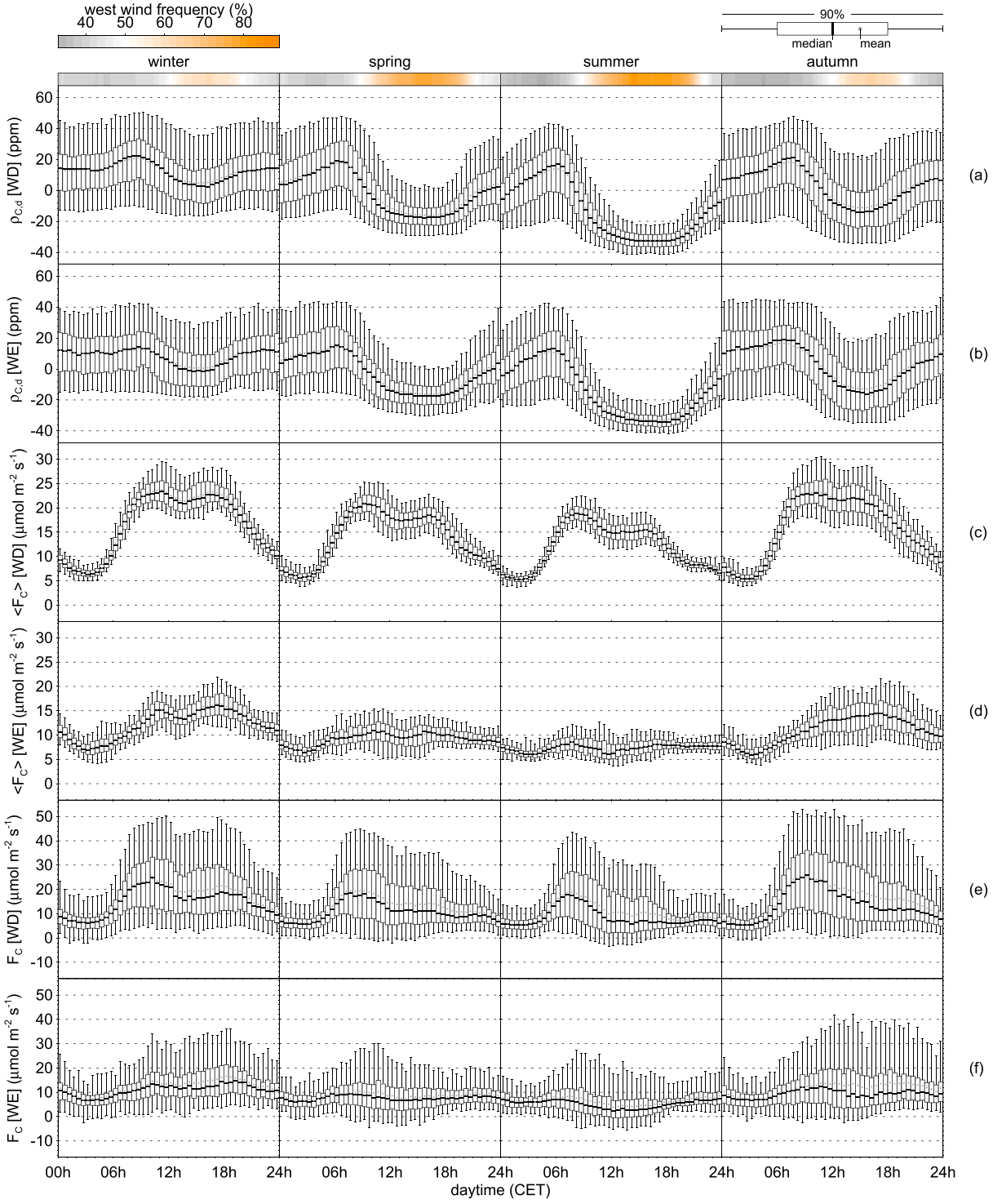

Figure 5. Mean seasonal diurnal courses of (a and b) ρ_C, (c and d) $<F_C>$, and (e and f) F_C from 2005 to 2014. Columns represent different seasons. Variables are presented for weekdays (WD) as well as weekends (WE). The bar on top of plot indicates frequency of west wind. The boxplots show the 5th, 25th, 75th, and 95th percentiles as well as the mean and the median of the data. Note the difference in *y* axis scale between Figures 5c and 5d and Figures 5e and 5f.

NW winds are subject to the nighttime and daytime parts of the mountain-valley system of the Rhine valley, respectively. While the general wind regime is very persistent, the ESE component occurs more often during day in autumn and winter and the W/NW component is typically more frequent in spring and summer. Average wind speed is 2.4 m s^{-1} ± 1.2, whereas stronger wind speeds are normally related to the western sector.

The local wind system with its diurnal behavior is crucial to the measurement of F_C as the wind direction determines, which sources actively contribute to the measured signal. In the morning, high CO_2 emissions are advected from the Klingelbergstrasse in the east, resulting in high F_C, whereas in the afternoon, when the west winds advect emission from the residential sector, measured F_C is relatively low. Only between October and February, when the ESE component is more persistent during the day, afternoon traffic or the evening rush hour is clearly represented by the measurements (Figures 5e and 5f). The calculation of horizontal averages compensates for this effect.

3.2. Carbon Dioxide Footprint Estimation

Footprints for F_C were calculated from 30 min data according to *Kormann and Meixner* [2001], which is an analytical footprint model for nonneutral stratification. To run the model the displacement height z_d and the roughness height z_0 were derived by the rule of thumb $z_d = 2/3\ z_h$ and $z_0 = 0.1\ z_h$, respectively, where z_h is the mean building height (16.6 m) derived from the 3-D city model. For an estimation of source area seasonality, average source areas were calculated for single seasons and years from the 30 min footprints. The overall average footprint is shown in Figure 1 for a domain of 1.6×1.6 km. The general shape of the footprint contour lines compares well with the characteristic east-west distribution of the wind rose (Figure 4). A strong SE component and a rather diffuse west branch are characteristic for the source area. The footprint extends at its maximum 500 m (east), but typically ranges within 300–400 m (90% contours). The general shape of the footprint is preserved over the year, because of the persistent daily wind regime. Nevertheless, between single years and especially between seasons characteristic differences can be distinguished. The area within the 90% contours is largest during winter with 0.74 km^2 and smallest in autumn with 0.57 km^2 (−23.3%), whereas during spring and summer the footprint covers 0.70 km^2 (−5.3%) and 0.60 km^2 (−19.1%), respectively. The differences in footprint size are primarily subject to the varying strength of the eastern branch of the footprint area, which extends the most in winter, followed by autumn, spring, and summer. The variation of the western part is smaller, except for the autumn situation, where less of the residential area to the northwest is covered. From a larger footprint area a well-mixed signal with fewer contributions of single nearby sources can be assumed. The footprint defines which sources and sinks actively contribute to the measured, and thus, a variation in the source area can directly affect the measured pattern, especially in a heterogeneous urban environment.

3.3. The Impact of Horizontal Averaging on Sectorial CO_2

To quantify the impact of horizontal averaging on the total carbon (C) balance, average yearly cumulative fluxes nC and $<nC>$ were calculated from the EC data. Due to the inaccuracy of C storage estimations from single point measurements, the storage term ΔC_S was not calculated for the derivation of net ecosystem exchange values. From street canyon profile measurements in London, UK, *Bjorkegren et al.* [2015] have shown that the impact of ΔC_S on F_C is typically less than 1% of the magnitude of the vertical flux during well-mixed conditions and diurnal and seasonal patterns are not altered significantly. nC is a good indicator to reveal the heterogeneity of the source/sink distribution within the surrounding of the BKLI site as well as the unequally distributed occurrence of different wind directions. Both F_C and nC are affected significantly by the horizontal averaging procedure, but the effect on nC is much larger. While the frequency of occurrence of a sector does not directly affect the magnitude of F_C, nC is very sensitive to the distribution of wind directions. Changes in F_C are thus more related to the unequal frequency distribution of daytime and nighttime values and different seasons recorded for each sector. Sectorial values of F_C and nC as well as $<F_C>$ and $<nC>$ are shown in Figure 6. Horizontal averaging leads to increased F_C for sectors 4 through 7 and clearly smaller fluxes for sectors 1 through 3 and sector 8. Largest changes are observed for sector 2 (−12.8%) and sector 5 (+12.8%). Changes for nC are much larger, especially for the frequent sector 4, where nC is reduced by −116%. Compared to nC, $<nC>$ clearly better reflects the sectorial CO_2 balance represented by $<F_C>$ in Figure 6b. The different weighting of individual sectors by horizontal averaging leads to an average $<F_C>$ of 13.3 $\mu mol\,m^{-2}\,s^{-1}$ (+7.6%) compared to the directly measured F_C of 12.3 $\mu mol\,m^{-2}\,s^{-1}$. The increase in nC is of the same order of magnitude from 4.6 to 4.9 $kg\,C\,m^{-2}\,yr^{-1}$ (+6.5%).

3.4. Long-Term Time Series of CO_2 Mixing Ratio

3.4.1. Diurnal Cycles and Yearly Variability

Mean diurnal cycles of ρ_C were calculated from 30 min averages. Influences of long-term trends have been removed from the time series by subtracting the linear trend calculated over the past 10 years from each

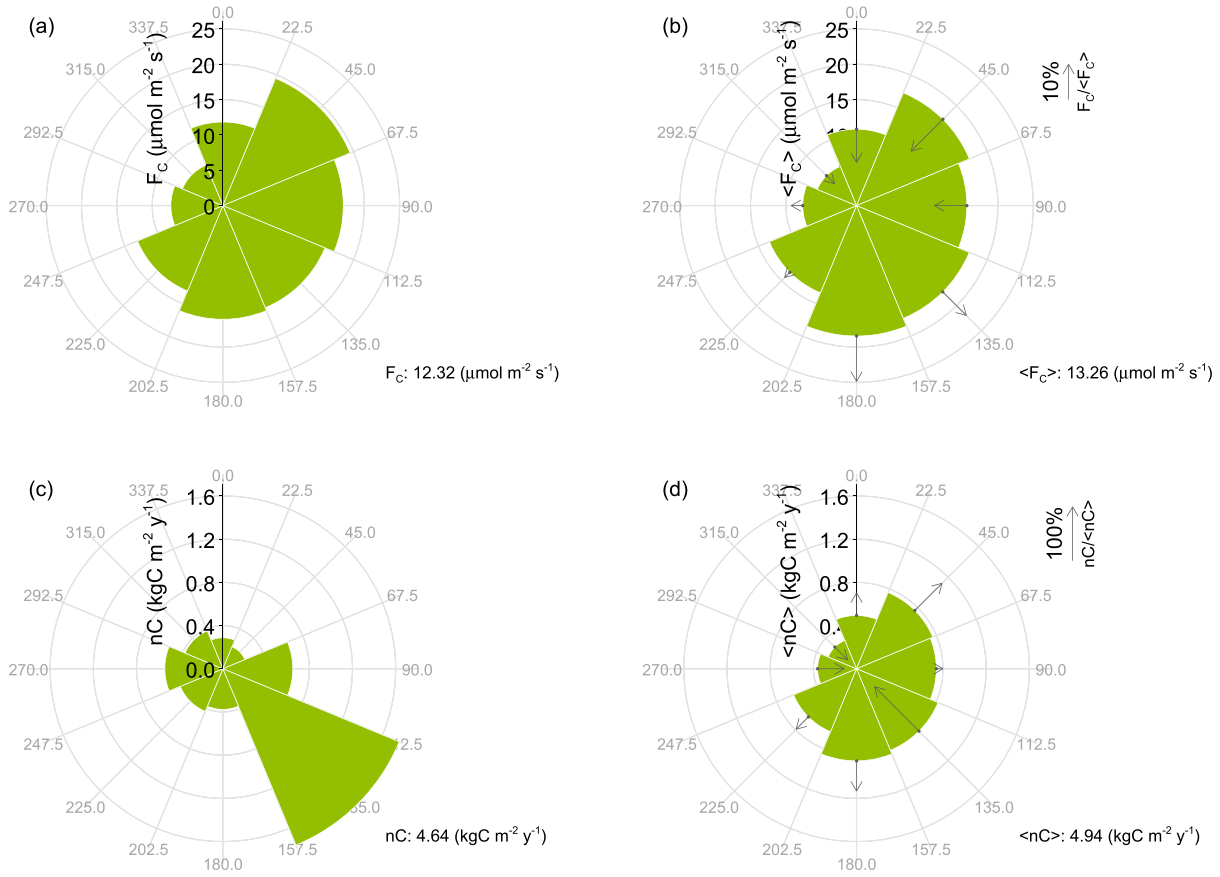

Figure 6. Average annual (a) F_C, (b) $<F_C>$, (c) nC, and (d) $<nC>$ per sector between 2005 and 2014. The arrows in Figures 6b and 6d indicate relative effect of horizontal averaging on F_C and nC, respectively.

value ($\rho_{C,d}$). Diurnal courses split by seasons are plotted in Figure 5a for weekdays and Figure 5b for weekends. Besides the impacts of surface sources and sinks, the diurnal variability of $\rho_{C,d}$ is by large parts controlled by the dynamics of the convective mixed layer [*Reid and Steyn*, 1997]. Because the mole fraction of CO_2 is inversely correlated to the air volume in the boundary layer (BL) top, highest values are measured in the shallow early morning BL between 05:00 and 07:00. With increasing turbulence after sunrise $\rho_{C,d}$ continuously decreases until minima values are reached around 15:00 at the BKLI site. After sunset, when the BL height decreases, $\rho_{C,d}$ increases steadily during the night. The daily amplitude (A_D), calculated as the average peak to trough difference, ranges from 16.4 ppm in winter to 46.2 ppm in summer. The average A_D is 31.5 ppm, although on individual diurnal cycles the variability around the mean can be large as indicated by the boxplots in Figures 5a and 5b. Results from similar measurements are reported by *Grimmond et al.* [2002] for Chicago (35 ppm (summer), 13 days), by *Reid and Steyn* [1997] for Vancouver (27 ppm (June), 11 days), by *Vogt et al.* [2005] for Basel (61 ppm (June/July), 28 days), and by *Moriwaki and Kanda* [2004] for Kugahara, Tokyo (10 ppm (July), 20 ppm (December), 1 year). Nevertheless, these studies are all very short ranging and thus hardly comparable to the present data set. For the EGH site nearby London a representative average daily amplitude of 17 ppm was calculated by *Hernández-Paniagua et al.* [2015] from data between 2000 and 2012, which is clearly below BKLI because the EGH site located 32 km outside the dense urban center of London. The general diurnal behavior of ρ_C is also reported in several other studies from (sub)urban environments [*Coutts et al.*, 2007; *Crawford and Christen*, 2014; *Lietzke and Vogt*, 2013; *Velasco et al.*, 2005], but comparable results from multiyear studies are rare.

The average diurnal courses clearly indicate that during winter the morning maxima occur later and the increase in the late afternoon starts earlier as a direct result of the shorter period of daylight. The wintertime daily average mole fraction is roughly 25 ppm higher compared to summer because (i) during winter the UBL

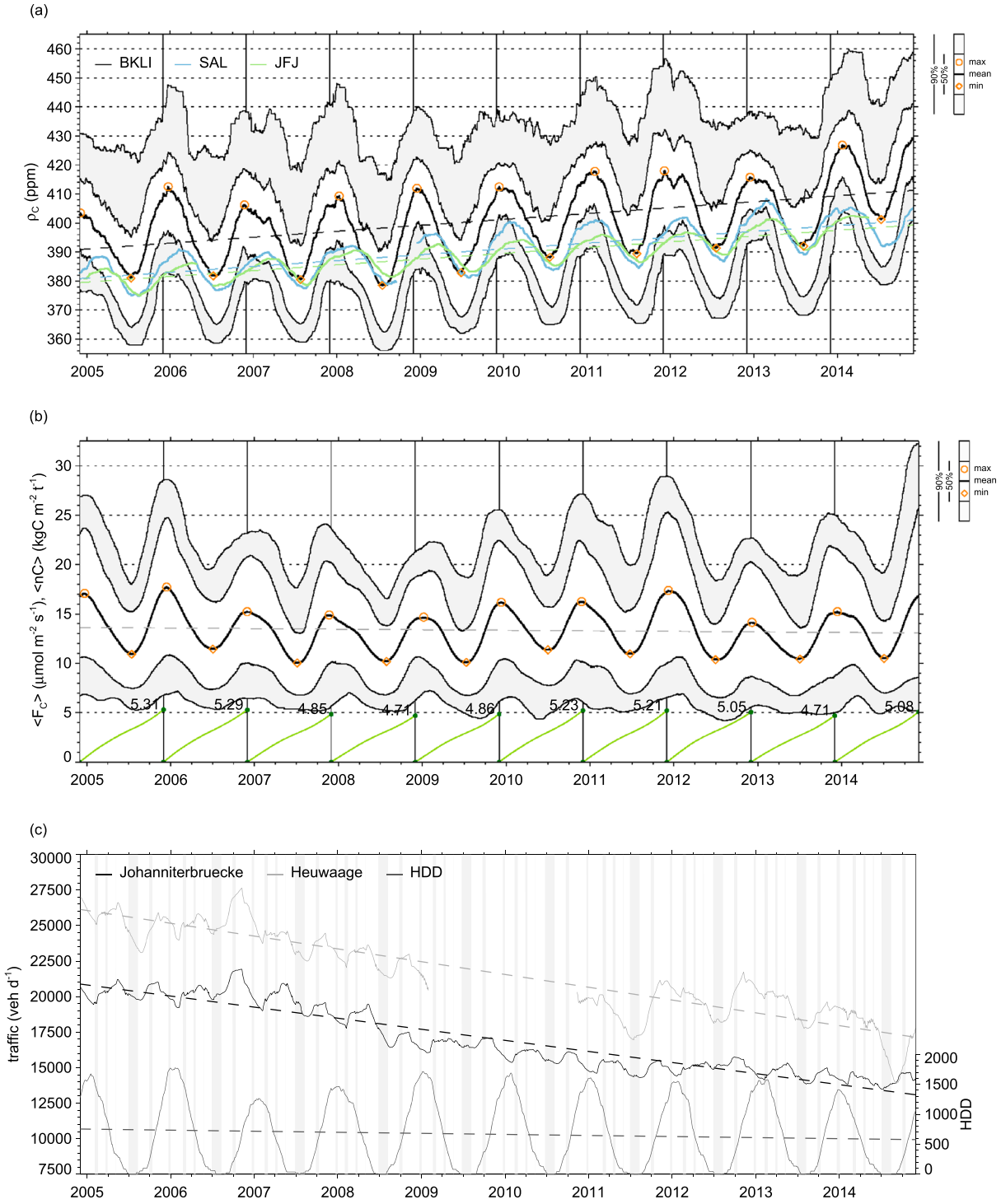

Figure 7. (a) Time series of ρ_C at BKLI, Schauinsland (SAL), and Jungfraujoch (JFJ) and (b) time series of $<F_C>$ and yearly cumulative $<nC>$ (green lines) and (c) traffic count as well as HDD from 2005 until 2014. The solid lines are 90 days running means of half hourly data. Statistics for BKLI are indicated by grey shaded areas. The dashed lines show the linear regression for each time series. Additionally, winter maxima (circles) and summer minima (diamonds) are drawn. The grey shaded areas in Figure 7c indicate public and school holidays.

is generally stratified less unstable, (ii) additional CO_2 is emitted from anthropogenic sources, and (iii) uptake by photosynthesis is mostly inactive. This difference can be as high as 40 ppm during the day, but almost vanishes in the early morning. If weekdays are compared to weekends, $\rho_{C,d}$ is reduced by 3.4 ppm (winter), 1.8 ppm (spring), 0.8 ppm (summer), and 0.4 ppm (autumn) during weekends. Thus, the variation in direct

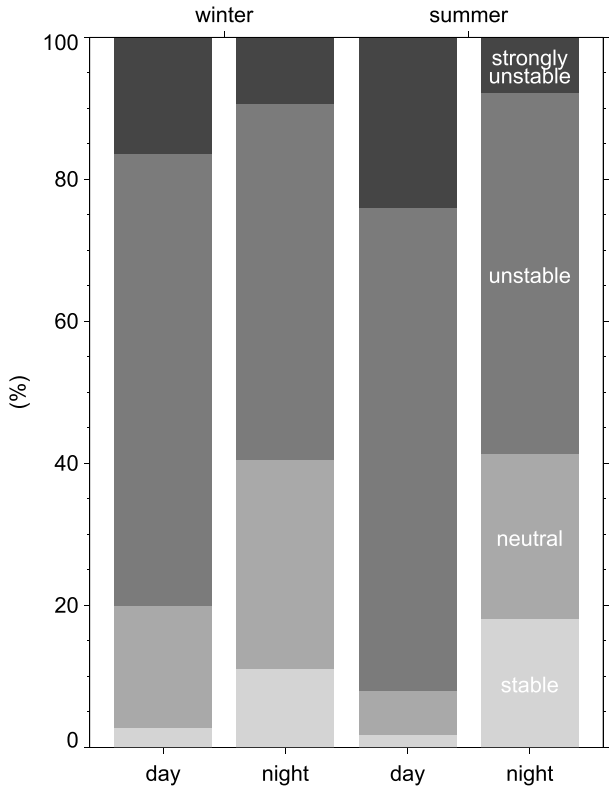

Figure 8. Relative frequency of stability classes split by winter and summer as well as day and night (separated by shortwave radiation data). Stable $\zeta > 0.05$, neutral $0.05 > \zeta >$ -0.05, weakly unstable $-0.05 > \zeta > -1.0$, and unstable $\zeta < -1.0$. The stability index represents $(z - z_d)/L$, where L is the Obukhov length.

CO_2 emissions from, e.g., traffic only contributes little to the absolute mole fraction of CO_2, and the impact of the BL dynamics and uptake by vegetation is of much higher importance for the variability of $\rho_{C,d}$ on daily and seasonal scales. The statistics in Figures 5a and 5b also indicate that the variability within the 10 years is smallest during the day in spring and in summer but nearly the same during nighttime for all seasons. The larger mixing volume during summer and spring days seems to prevent large variations in ρ_C, whereas in the shallow nocturnal BL changes in ρ_C occur more rapidly.

3.4.2. Long-Term Trend and Seasonal Patterns

For the analysis of long-term trends in ρ_C the time series was smoothed by applying a 90 day running mean filter to the 30 min data (Figure 7a). For comparison, high-accuracy CO_2 samples from Global Atmosphere Watch (GAW) stations at Schauinsland (SAL, 40 km northward, 1205 m above sea level (asl) [*Luftmessnetz des Umweltbundesamtes*, 2015]) and Jungfraujoch (JFJ, 120 km southward, 3580 m asl [*University of Bern*, 2015]) are considered. While BKLI represents the local urban BL, SAL acts as a regional background only partially influenced by local sources depending on the vertical BL extension and JFJ gives information about the free atmosphere. Like this these three stations are considered as a quasi-vertical transect through the lower troposphere. The residual after filtering the data reveals the typical seasonal patterns with highest values during winter and lowest values during summer, which has also been reported by several studies for different urban environments [*Hernández-Paniagua et al.*, 2015; *Lietzke et al.*, 2015; *Park et al.*, 2014; *Strong et al.*, 2011; *Valentino et al.*, 2008]. The driving mechanisms of the seasonal course of ρ_C are basically the same as those responsible for the daily cycle. During the day in winter time the mixed BL at BKLI is generally less developed indicated by the shift of stability toward less unstable conditions (Figure 8). Thus, higher ρ_C values partly result from the smaller mixing volume. On the other hand, during the night, differences in the stability regime between summer and winter are negligible and the frequency of stable conditions during summer is even higher at the expense of less neutral stratification. This explains, why the early morning maximum peak of ρ_C does not vary that much between season compared to the differences in the afternoon minimum (Figures 5a and 5b). Additionally, the seasonal differences are enforced due to the varying CO_2 uptake by vegetation in summer and winter, but the influence of photosynthetic CO_2 uptake cannot be determined quantitatively for the BKLI site.

The seasonal behavior of the BKLI data coincides well with the patterns observed at the regional background. The course of the BKLI measurements shows more short-term variability, and the seasonal shape is less marked, especially during the winter, which highlights that the urban BL encounters more variation in source/sink distribution and atmospheric conditions than the overlying lower troposphere. The long-term trend, calculated as the linear regression from 30 min data, emphasizes the long-term increase in ρ_C observed on a global scale [*Tans and Keeling*, 2015]. Over the last 10 years the slope is 1.98 ppm yr^{-1} at BKLI, which compares well to the values calculated for SAL (1.97 ppm yr^{-1}) and JFJ (1.98 ppm yr^{-1}). For the EGH site near

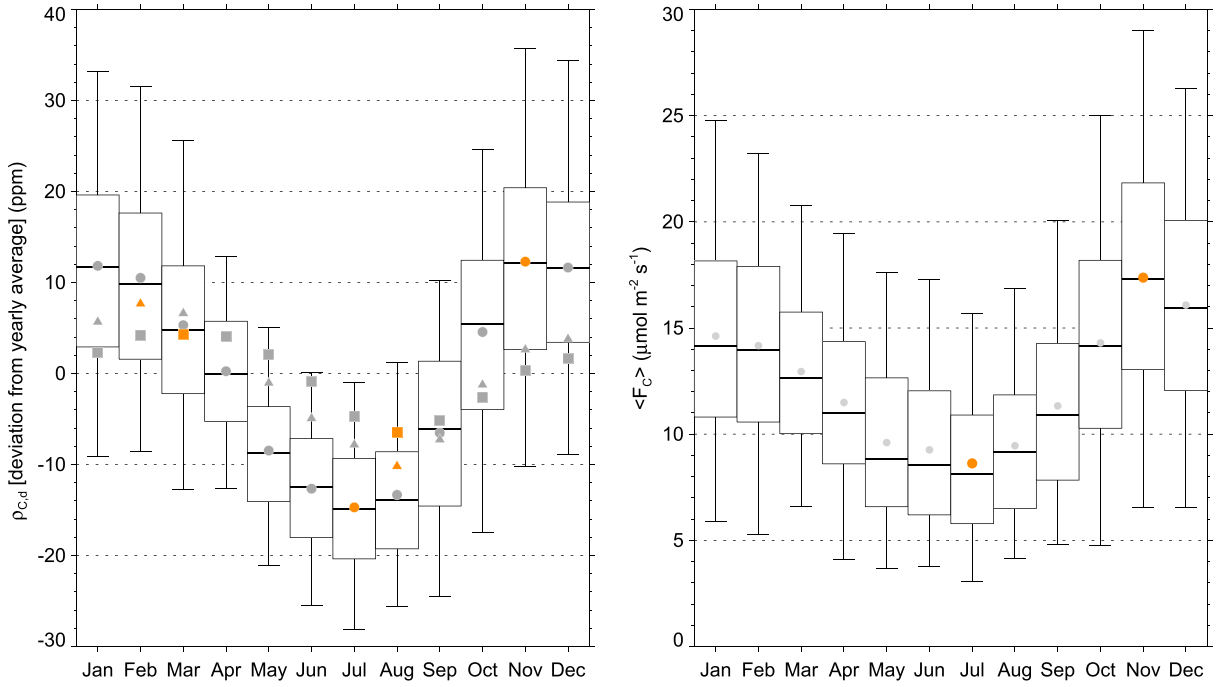

Figure 9. (left) Average seasonal amplitude (deviation from yearly mean) of ρ_C for BKLI (circle), SAL (triangles), and JFJ (squares) and (right) average seasonal amplitude of $<F_C>$ at BKLI. Depicted are average monthly values of $\rho_{C,d}$ calculated from daily averages corrected for long-term trend of each station. Winter and summer peak values are marked orange. Boxplots as in Figure 5.

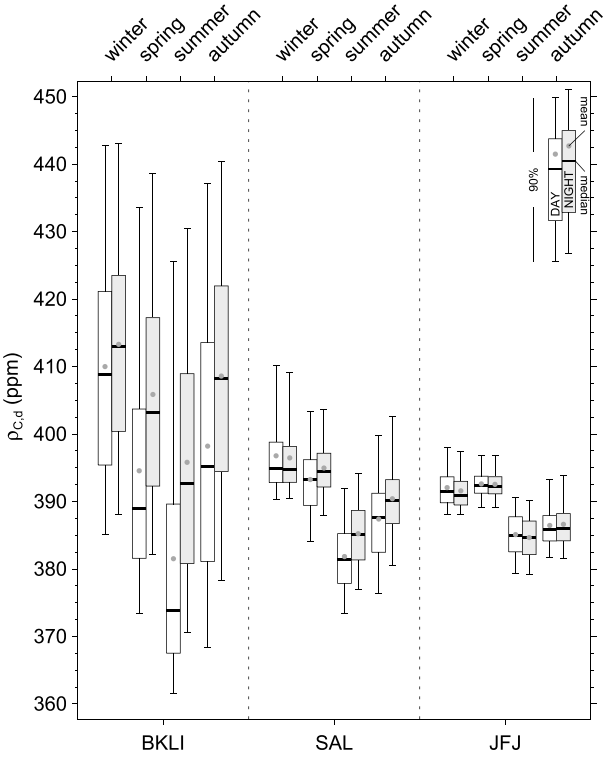

Figure 10. Average seasonal daytime and nighttime $\rho_{C,d}$ for BKLI, SAL, and JFJ. Values are corrected for long-term trend, and the long-term mean is added afterward.

London *Hernández-Paniagua et al.* [2015] report 2.5 ppm yr^{-1} for the period between 2000 and 2012, and the most recent IPPC report [*IPCC*, 2013] specifies a global trend of 2.0 ppm yr^{-1} between 2001 and 2013 calculated from Mauna Loa and South Pole data.

Even though the secular trend reveals that regional and local ρ_C is interconnected concerning long-term trends, the variation in local ρ_C can be large. The year-to-year growth rate at BKLI, for example, varies from −1.7 ppm yr^{-1} (2006 to 2007) to 4.6 ppm yr^{-1} (2010 to 2011) and was unexceptionally high from 2013 to 2014 with 13.4 ppm yr^{-1}. Nevertheless, the average yearly growth rate is 2.6 ppm yr^{-1} and thus of the same order of magnitude than the calculated linear trend which led to an increase in ρ_C from 393.8 ppm in 2005 up to 417.0 ppm in 2014. Since 2010, the average yearly ρ_C never dropped below the 400 ppm margin again.

The average seasonal drop of ρ_C from winter mean to summer mean is 22.0 ppm, and the average raise from summer mean

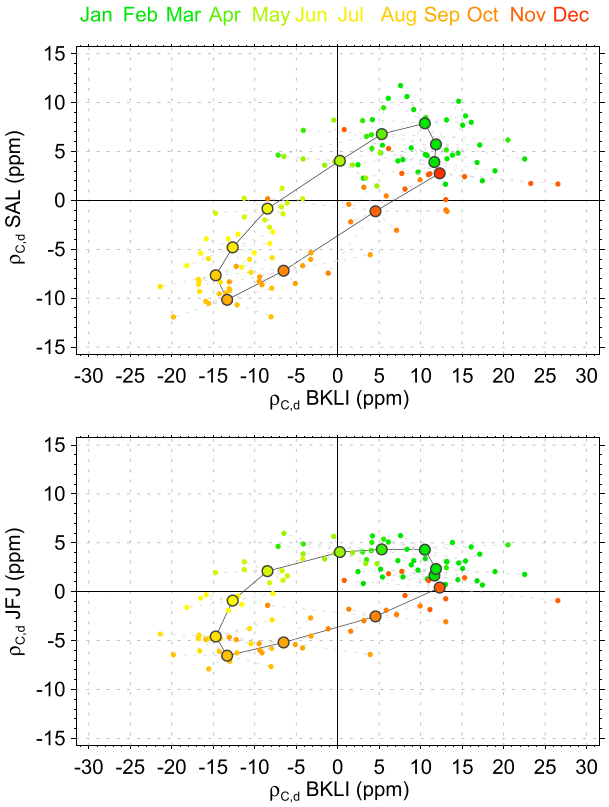

Figure 11. Hysteresis between detrended $\rho_{C,d}$ of (top) BKLI and SAL as well as (bottom) BKLI and JFJ. Depicted are monthly mean values (small dots) and average monthly values (large dots).

to winter mean is 24.9 ppm. The average peak to trough (Figure 7a) drop (max to min) and raise (min/max.) values are slightly higher with 26.8 ppm and 29.5 ppm, respectively. For single years the seasonal drop and raise of ρ_C in spring can be as large as 25.7 ppm (2006) and 30.8 ppm (2013) or as low as 17.0 ppm (2005) and 19.1 ppm (2006). The average yearly course of ρ_C is visualized in Figure 9a by monthly mean values based on daily averages corrected for long-term trend. The seasonal amplitude is skewed, and the raise of ρ_C in autumn occurs faster than the drop in spring. During winter month the variability is slightly larger, which reflects the fact that ρ_C varies more in the shallow wintertime boundary layer due to the smaller mixing volume compared to the better mixed and more evolved boundary layer during summer month. The winter maxima at BKLI occur relatively regularly in late November or early December, whereas the summer minima appear between June and August. The variability in summertime peaks is generally larger ($\sigma = 2.1$ ppm, where σ is the standard deviation) compared to wintertime maximum values ($\sigma = 1.9$ ppm).

3.4.3. Coupling to Background CO_2 Mole Fraction

In Figure 10 average seasonal ρ_C split by season and day/night are shown for BKLI and JFJ. Compared to the regional and tropospheric background mole fraction BKLI shows on average an increased ρ_C of about 10 ppm (SAL) to 11.4 ppm (JFJ) as a result of the nearby strong surface sources of CO_2. While ρ_C always stays above background mole fraction during winter and autumn all the day and also in spring and summer during the night, daytime ρ_C during spring and summer is on average mixed down to the background mole fraction level. Indicated by the statistics in Figure 10, local ρ_C also very frequently drops below the background record. Even though plant uptake of CO_2 at BKLI might not be able to reduce ρ_C that much, the vertical stretching of the BL during the day and large-scale horizontal advection of air masses from the rural surrounding keep the mole fraction below the tropospheric level [*Helfter et al.*, 2011; *Strong et al.*, 2011].

Concerning summer and winter peak, local ρ_C clearly differs from the background record not only in absolute values but also in time when the maxima and minima values are measured during the year. On average ρ_C at BKLI peaks in late November or early December and summertime minima occur in June and July (Figure 7). In contrast ρ_C at SAL and JFJ peaks in February and March, respectively, and both have their minima sometime during August. Whereas the decadal trend and the similarity of seasonal patterns between BKLI, SAL, and JFJ already point toward a direct coupling between local and background ρ_C, the shift in peak refines this relationship. The average exchange between the local BL and the troposphere follows a hysteresis with a delay of up to 3 months in winter and at least 1 month in summer. The hysteresis (Figures 11a and 11b) becomes more distinct with increasing distance to surface sources horizontally and vertically.

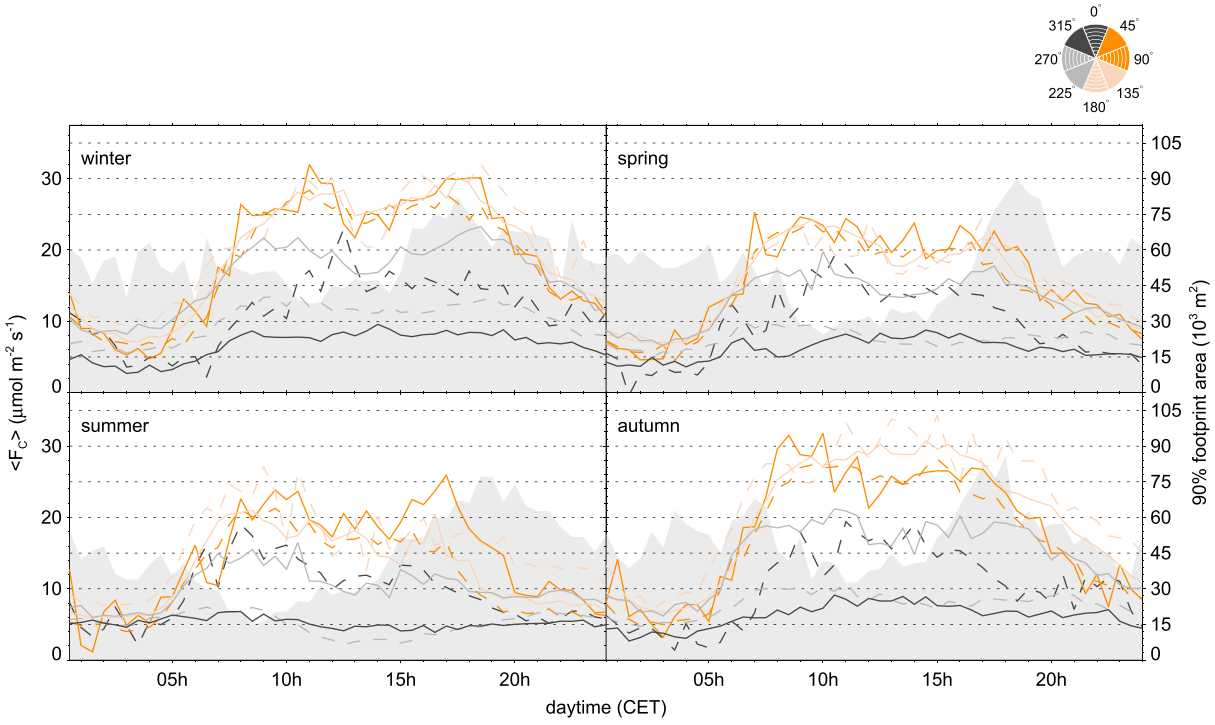

Figure 12. Average sectoral diurnal course of $<F_C>$ for each season. Additionally, the area covered by the 90% footprint contour line is indicated on the secondary *y* axis (grey shaded area).

3.5. Long-Term Time Series of CO_2 Flux

3.5.1. Diurnal Course and Yearly Variability of $<F_C>$

Average diurnal courses of $<F_C>$ were derived from 30 min data separated by season and weekday/weekend (Figures 5c and 5d). Generally, the diurnal course of $<F_C>$ follows the daily dynamic of the traffic. The direct relationship between $<F_C>$ and the diel cycle of traffic has already been reported by a number of studies qualitatively [*Coutts et al.*, 2007; *Moriwaki and Kanda*, 2004; *Song and Wang*, 2012; *Vogt et al.*, 2005] and quantitatively [*Lietzke and Vogt*, 2013; *Velasco et al.*, 2005]. Both traffic and $<F_C>$ follow a dual peaked pattern with minimum values in the early morning and two maxima corresponding to the morning and evening rush hour. Between the rush hours there is a depression at noon. The two peaks of $<F_C>$ relating to the two rush hours around 08:00–09:00 in the morning and 16:00–17:00 in the afternoon are apparent during all seasons. Nevertheless, the afternoon peak in $<F_C>$ is slightly reduced in spring and summer. If sectorial diurnal courses of $<F_C>$ are considered for different seasons (Figure 12) it becomes clear that the smaller afternoon peak is persistent for all wind directions in spring and summer and is thus not a direct function of wind direction. Figure 12 additionally shows the average diurnal course of the calculated footprint area (90% contour line) for each season. Generally, the footprint extends the most in afternoon and shows a minimum between 06:00 and 12:00 in the morning. The diurnal course is less developed in autumn and winter but shows a very distinct shape during spring and summer. The larger footprint in the afternoon, mainly caused by higher wind speed, results in smaller CO_2 fluxes because the additional extent of the footprint area damps the impact of the strong nearby traffic source and leads to a better mixed CO_2 input. During autumn and winter additional sources are active due to heating activity; thus, the footprint size does not affect the CO_2 signal the same. Still, also during the winter months a damping effect on the afternoon peak is observable, if the fact is taken into account that the evening traffic rush hour is more intensive compared to the morning traffic peak.

All over the year, lowest fluxes are measured in the early morning (03:00–04:00) with 5–6 $\mu mol\,m^{-2}\,s^{-1}$. This is when traffic volume, heating activity, and human activity, in general, are lowest. The daily minimum is also consistent for weekdays and weekends. Thus, the base load of the CO_2 emissions of the urban metabolism at BKLI seems to prohibit $<F_C>$ dropping below the threshold of approximately 5 $\mu mol\,m^{-2}\,s^{-1}$ on average.

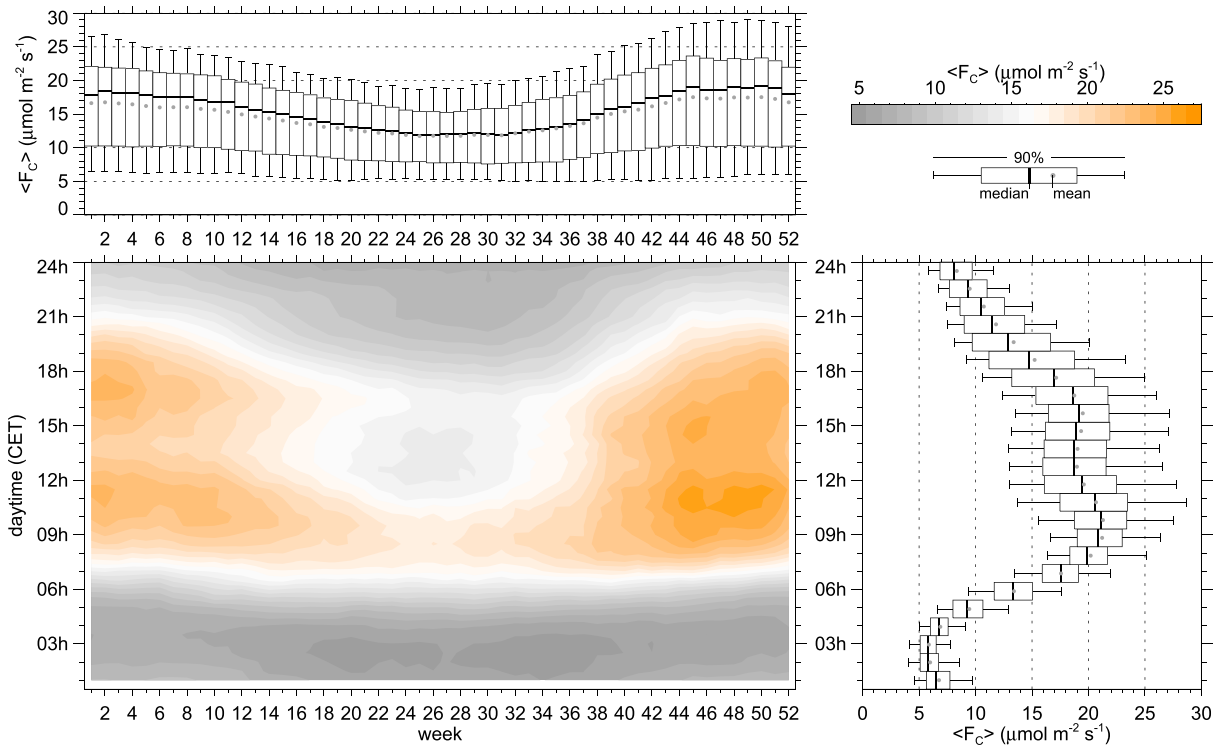

Figure 13. Isopleth diagram for 7 day bins of $<F_C>$ with (top) average seasonal and (right) average diurnal courses. Color levels indicate steps of 1 µmol m^{-2} s^{-1}.

Highest values usually occur during the morning rush hour ranging between 20–25 µmol m^2 s^{-1} in winter/autumn and 15–20 µmol m^{-2} s^{-1} in summer. Average daily values reach from 11.2 µmol m^{-2} s^{-1} in summertime to 16.6 µmol m^{-2} s^{-1} during the winter month, and the variability during winter and autumn is larger ($\sigma = 1.42$ and $\sigma = 1.29$) compared to spring and summer ($\sigma = 0.6$ and $\sigma = 0.64$). Generally, the interannual variability is lower during periods with lower activity of CO_2 sources (summer, nighttime). On average, positive values are recorded for all seasons and all years, which accentuates that CO_2 uptake by photosynthesis is too weak to completely offset the CO_2 emissions. Minor effects of photosynthetic activity can be observed for sectors 6 and 7, where the daytime $<F_C>$ slightly drops below the nocturnal values during summer (Figure 12). The seasonal pattern of the diurnal course of $<F_C>$ is depicted in Figure 13 also by an isopleth diagram. Especially, in the morning, one can recognize that $<F_C>$ starts to increase earlier between weeks 13 and 43 as a result of the shift between daylight saving time and standard time. This highlights the direct influence of human activity on the diurnal course of CO_2.

3.5.2. Interannual Anomaly of CO_2

In Figure 7b a 90 day running mean filter was applied to $<F_C>$. Generally, $<F_C>$ follows a sinusoidal pattern with maximum values between 14.2 and 17.7 µmol m^{-2} s^{-1} during winter and minimum values between 10.0 and 11.4 µmol m^{-2} s^{-1} during summer. The variability of the winter time peak ($\sigma = 1.19$) is larger than the summer minima ($\sigma = 0.52$), and the interquartile range (IQR) also points out that variation in $<F_C>$ is generally larger during winter months (IQR ≈ 10–15 µmol m^{-2} s^{-1}) compared to summer month (IQR ≈ 5–8 µmol m^{-2} s^{-1}). The variability is only weakly represented by the lower quartile, whereas the upper quartile follows well the interannual differences both during winter and summer. The seasonal statistics reveal again that $<F_C>$ minima values occur around 5 µmol m^{-2} s^{-1}. This value is slightly higher during winter, when the base load of the city is on a higher level due to additional CO_2 emissions from heating activity and possibly plant respiration. Additionally, the seasonal course of $<F_C>$ shows again that photosynthetic activity is far from offsetting the CO_2 emissions. This is also observed in most other comparable urban environments, and only studies from vegetated suburban neighborhoods report clear offsetting effects by vegetation [*Bergeron and Strachan*, 2011; *Crawford et al.*, 2011; *Ramamurthy and Pardyjak*, 2011; *Velasco et al.*, 2013].

The seasonal amplitude of $<F_C>$ is on average 4.2 µmol m^{-2} s^{-1} ($\sigma = 0.95$) for the drop in spring and 4.1 µmol m^{-2} s^{-1} ($\sigma = 0.94$) for the raise in autumn. Large raise of $<F_C>$ in autumn is usually followed by large

drop in spring, because variability in winter maxima is much larger and $<F_C>$ always drops to similar values in summer. Peak dates of $<F_C>$ are comparable to those of ρ_C; thus, winter maxima are generally reached in early December, whereas the summertime minimum occurs around July. Winter peak dates are very consistent and vary only little. Summertime minima peak dates in contrast are scattered from late June until early August.

If temperature as a measure for heating activity is considered as the main driver for seasonal variation of $<F_C>$, the winter peaks occur unexpectedly early. If the yearly course of temperature is considered, minimum values are usually recorded in early January, which is approximately 1 month after the peak in $<F_C>$. Despite the fact that $<F_C>$ follows the seasonal course of air temperature, the relationship between $<F_C>$ and heating activity controlled by air temperature is not straightforward and has to be validated furthermore with, e.g., current energy consumption data. To demonstrate this issue, heating degree days (HDD) as a measure for heating activity are plotted in Figure 7c. Clearly, the maximum values are reached after New Year's Day in most occasions. From these values, peak date of $<F_C>$ is rather expected to occur in mid-January. The small footprints in autumn compared to the larger ones in winter possibly explain the relatively early peak of $<F_C>$. Accordingly, in autumn strong nearby CO_2 sources (e.g., Klingelbergstrasse) contribute more to $<F_C>$, whereas the larger footprint in winter leads to a generally better mixed CO_2 signal, because the relative contribution of point or linear sources decreases.

3.5.3. Secular Trends and Long-Term Behavior of $<F_C>$

Between 2005 and 2009 $<F_C>$ clearly shows a decrease, but this period is followed by 3 years of slightly higher fluxes. Following the linear trend calculated over the last 10 years $<F_C>$ is reduced by $-0.65\,\mu mol\,m^{-2}\,s^{-1}$. Even though the trend points toward the expected direction, it is surprisingly low. The analysis of the nearby traffic count data shows that due to the opening of the northern traffic bypass in 2007/2008, total traffic volume at BKLI was reduced by approximately 25% between 2005 and 2014 (Figure 7c). By comparison, $<F_C>$ was reduced by 4.7% within the same period. Even though the reduction in traffic volume seems to have a reducing effect on $<F_C>$, the correlation is relatively weak (not shown). This is in contrast to the very strong relations achieved by regression analysis of diurnal cycles of $<F_C>$ and traffic. The question then arises as to how far a single nearby traffic count is representative for the investigation area. From the current data, it seems as the shape of the diurnal cycle of $<F_C>$ is given by the increase and decrease of the traffic volume, but the absolute $<F_C>$ values are not solely controlled by direct traffic emissions.

First, the measured F_C is possibly composed of emissions not only from the nearby Klingelbergstrasse. Thus, the reduction of 25% in traffic volume is not necessarily valid for the whole road network within the footprint area. On a city scale traffic is actually not reduced but translocated. Additionally, changes in vehicle fleet composition and vehicle emission efficiency due to recent technologies are also influencing the CO_2 emissions but are difficult to account for and remain an uncertainty factor.

Second, the turbulent transport mechanisms from the source within the street canyon up to the measurement device are still not completely understood. For example, *Lietzke and Vogt* [2013] showed that at BKLI for east winds, in-canyon vortex structures work against the vertical transport, in contrast to west wind flows, where the vertical transport of air masses inside the canyon is enhanced. Due to these complex transport mechanisms, a linear relationship between emitted CO_2 or traffic volume and measured $<F_C>$ for all situations might be too simple. In addition, it is worth mentioning that while values of $<F_C>$ reported in literature (overview in *Lietzke et al.* [2015]) compare well between different sites, the corresponding traffic amounts do not reflect any simple correlation. There are many sites with measured $<F_C>$ far below the one at BKLI, but with 2 or 3 times the daily amount of traffic and vice versa.

Lastly, besides traffic volume other controlling factors (heating, vegetation, human activity, footprint variability etc.) are influencing the magnitude of $<F_C>$. Because these controlling factors do not implicitly show the same long-term trends, linear regressions from short investigation periods are not transferable to long-term time series.

4. Conclusions

This is the first study to present a full decade of urban CO_2 flux (F_C) measurements. The general long-term behaviors of CO_2 mole fraction (ρ_C) and F_C were analyzed from 10 years of open-path eddy covariance (EC)

measurements at the BKLI site between 2005 and 2014. So far, only little is known about the long-term trends of F_C in urban environments. Multiyear records of ρ_C and F_C are available for natural ecosystems, but rare for heterogeneous urban environments. Longest time series reported in literature cover at most 5–6 years, and thus, the analysis of the BKLI long-term data contributes substantially to the better understanding of seasonality and long-term variability of CO_2 in cities.

In contrast to relatively homogeneous footprints of natural ecosystems, the highly heterogeneous urban area increases the requirements for data post processing in order to achieve reliable and comparable results. Besides well-known processing steps for big data like gap-filling, our study proved the necessity of horizontal averaging for F_C to minimize effects of heterogeneous distribution in time and space of sources and sinks around the measurement site as well as the impact of changing diurnal and seasonal wind system. Another main advantage of horizontal averaging is that the comparability of data sets from different measurement sites can be improved considerably, because site-specific properties like wind system and source distribution are properly weighted and thus less influencing the variability factors of F_C.

The analysis of long-term ρ_C in the urban environment of Basel reveals good consistency with background concentration measurements at GAW stations (Schauinsland and Jungfraujoch), both in terms of seasonality and long-term trend (+2 ppm yr^{-1}). Between local and background ρ_C a phase shift of up to 3 months in winter and around 1 month in summer is observable. This can be explained by the time needed to mix the CO_2 from local near-surface air masses to the lower troposphere. The different time scales of this mixing process in winter and summer result from the varying mixing conditions in the boundary layer over the year. Being aware that it is not the intended purpose of open-path gas analyzers to deliver high-accuracy absolute CO_2 concentration measurements, the results of this study clearly prove a sufficiently high data quality to perform general trend analysis and detailed investigations on daily, seasonal, and even annual scales in urban environments.

Apart from typical diurnal, weekly, and seasonal features the current data give new insights into the temporal patterns and the variability of F_C also on interannual time scales. The relationship between F_C and human activity in urban areas is apparent due to distinct differences between weekday and weekend fluxes, the characteristic dual-peak diurnal course as a result of daily traffic volume, as well as the seasonality which is primarily caused by additional heating activity in winter. The variability of F_C is largest in times of high source activity during the day and especially in winter, but nearly vanishes e.g., in early morning, when most CO_2 sources show the lowest activity. Even though traffic volume was declining during the last decade, F_C was only reduced by roughly 5%. Clearly, the short-term variabilities in time and space caused by the highly heterogeneous environment and the local meteorology are superimposing any long-term tendency happening on much smaller scales.

Generally, the applicability of the EC method in heterogeneous urban environments is supported, even though basic theoretical requirements like stationarity or horizontal homogeneity are rarely fulfilled. But still, too few time series are available yet, which would be absolutely necessary as a solid data base for the increasing number of modeling approaches reported in literature as well as for intercomparisons of observed long-term pattern using horizontal averaging.

Acknowledgments
Research leading to this paper received funding from the project "Urban Climate Study of Bucharest" (IZERZ0_142160) made possible by the Romanian-Swiss Research Program. Special thanks go to the local authorities of Basel for open access to geospatial statistics and GIS data; the Luftmessnetz des Umweltbundesamtes, Germany, and the University of Bern, Switzerland, for providing the GAW data; as well as to Björn Lietzke for proofreading. The data used are listed in the references or available from the MCR-Lab on request (mi.schmutz@unibas.ch).

References

Aubinet, M., T. Vesala, and D. Papale (2012), *Eddy Covariance a Practical Guide to Measurement and Data Analysis*, Springer, New York, doi:10.1007/978-94-007-2351-1.

Bergeron, O., and I. B. Strachan (2011), CO_2 sources and sinks in urban and suburban areas of a northern mid-latitude city, *Atmos. Environ.*, *45*(8), 1564–1573, doi:10.1016/j.atmosenv.2010.12.043.

Bjorkegren, A. B., C. S. B. Grimmond, S. Kotthaus, and B. D. Malamud (2015), CO_2 emission estimation in the urban environment: Measurement of the CO_2 storage term, *Atmos. Environ.*, *122*, 775–790, doi:10.1016/j.atmosenv.2015.10.012.

Christen, A. (2005), Atmospheric turbulence and surface energy exchange in urban environments: Results from the Basel Urban Boundary Layer Experiment (BUBBLE), in *Stratus*, edited by E. Parlow, 142 pp., Univ. of Basel, Basel, Switzerland, doi:10.5451/unibas-003631734.

Christen, A. (2014), Atmospheric measurement techniques to quantify greenhouse gas emissions from cities, *Urban Clim.*, *10*, 241–260, doi:10.1016/j.uclim.2014.04.006.

Christen, A., N. C. Coops, B. R. Crawford, R. Kellett, K. N. Liss, I. Olchovski, T. R. Tooke, M. van der Laan, and J. A. Voogt (2011), Validation of modeled carbon-dioxide emissions from an urban neighborhood with direct eddy-covariance measurements, *Atmos. Environ.*, *45*(33), 6057–6069, doi:10.1016/j.atmosenv.2011.07.040.

Contini, D., A. Donateo, C. Elefante, and F. M. Grasso (2012), Analysis of particles and carbon dioxide concentrations and fluxes in an urban area: Correlation with traffic rate and local micrometeorology, *Atmos. Environ.*, *46*, 25–35, doi:10.1016/j.atmosenv.2011.10.039.

Coutts, A. M., J. Beringer, and N. J. Tapper (2007), Characteristics influencing the variability of urban CO_2 fluxes in Melbourne, Australia, *Atmos. Environ.*, *41*(1), 51–62, doi:10.1016/j.atmosenv.2006.08.030.

Crawford, B., and A. Christen (2014), Spatial variability of carbon dioxide in the urban canopy layer and implications for flux measurements, *Atmos. Environ.*, *98*, 308–322, doi:10.1016/j.atmosenv.2014.08.052.

Crawford, B., C. S. B. Grimmond, and A. Christen (2011), Five years of carbon dioxide fluxes measurements in a highly vegetated suburban area, *Atmos. Environ.*, *45*(4), 896–905, doi:10.1016/j.atmosenv.2010.11.017.

Falge, E., et al. (2001), Gap filling strategies for defensible annual sums of net ecosystem exchange, *Agric. For. Meteorol.*, *107*(1), 43–69, doi:10.1016/S0168-1923(00)00225-2.

Feigenwinter, C., R. Vogt, and A. Christen (2012), Eddy covariance measurements over urban areas, in *Eddy Covariance a Practical Guide to Measurement and Data Analysis*, edited by M. Aubinet, T. Vesala, and D. Papale, pp. 377–397, Springer, New York, doi:10.1007/978-94-007-2351-1_16.

Foken, T., and B. Wichura (1996), Tools for quality assessment of surface-based flux measurements, *Agric. For. Meteorol.*, *78*(1–2), 83–105, doi:10.1016/0168-1923(95)02248-1.

Foken, T., M. Göckede, M. Mauder, L. Mahrt, B. Amiro, and W. Munger (2005), Post-field data quality control, in *Handbook of Micrometeorology*, vol. 29, pp. 181–208, Kluwer Acad., New York, doi:10.1007/1-4020-2265-4_9.

Geodaten Kanton Basel-Stadt (2015), Grundbuch- und Vermessungsamt, Fachstelle für Geoinformation, Switzerland. [Available at http://www.geo.bs.ch/.]

Gioli, B., P. Toscano, E. Lugato, A. Matese, F. Miglietta, A. Zaldei, and F. P. Vaccari (2012), Methane and carbon dioxide fluxes and source partitioning in urban areas: The case study of Florence, Italy, *Environ. Pollut.*, *164*, 125–131, doi:10.1016/j.envpol.2012.01.019.

Göckede, M., et al. (2007), Quality control of CarboEurope flux data Part I: Footprint analyses to evaluate sites in forest ecosystems, *Biogeosci. Discuss.*, *4*(6), 4025–4066, doi:10.5194/bgd-4-4025-2007.

Grimmond, C. S. B., T. S. King, F. D. Cropley, D. J. Nowak, and C. Souch (2002), Local-scale fluxes of carbon dioxide in urban environments: Methodological challenges and results from Chicago, *Environ. Pollut.*, *116*(Suppl.1), S243–S254, doi:10.1016/S0269-7491(01)00256-1.

Helfter, C., D. Famulari, G. J. Phillips, J. F. Barlow, C. R. Wood, C. S. B. Grimmond, and E. Nemitz (2011), Controls of carbon dioxide concentrations and fluxes above central London, *Atmos. Chem. Phys.*, *11*(5), 1913–1928, doi:10.5194/acp-11-1913-2011.

Hernández-Paniagua, I. Y., D. Lowry, K. C. Clemitshaw, R. E. Fisher, J. L. France, M. Lanoisellé, M. Ramonet, and E. G. Nisbet (2015), Diurnal, seasonal, and annual trends in atmospheric CO_2 at southwest London during 2000–2012: Wind sector analysis and comparison with Mace Head, Ireland, *Atmos. Environ.*, *105*, 138–147, doi:10.1016/j.atmosenv.2015.01.021.

Hofmann, D. J., J. H. Butler, and P. P. Tans (2009), A new look at atmospheric carbon dioxide, *Atmos. Environ.*, *43*(12), 2084–2086, doi:10.1016/j.atmosenv.2008.12.028.

Intergovernmental Panel on Climate Change (IPCC) (2013), *Climate Change 2013: The Physical Science Basis. Contribution of Working Group I to the Fifth Assessment Report of the Intergovernmental Panel on Climate Change*, 1535 pp., Cambridge Univ. Press, Cambridge, U. K., doi:10.1017/CBO9781107415324.

Intergovernmental Panel on Climate Change (IPCC) (2014), *Climate Change 2014: Mitigation of Climate Change. Contribution of Working Group III to the Fifth Assessment Report of the Intergovernmental Panel on Climate Change*, Cambridge Univ. Press, Cambridge, U. K.

Kormann, R., and F. X. Meixner (2001), An analytical footprint model for non-neutral stratification, *Boundary Layer Meteorol.*, *99*(2), 207–224, doi:10.1023/a:1018991015119.

Lietzke, B., and R. Vogt (2013), Variability of CO_2 concentrations and fluxes in and above an urban street canyon, *Atmos. Environ.*, *74*, 60–72, doi:10.1016/j.atmosenv.2013.03.030.

Lietzke, B., R. Vogt, C. Feigenwinter, and E. Parlow (2015), On the controlling factors for the variability of carbon dioxide flux in a heterogeneous urban environment, *Int. J. Climatol.*, doi:10.1002/joc.4255.

Liu, M., J. Wu, X. Zhu, H. He, W. Jia, and W. Xiang (2015), Evolution and variation of atmospheric carbon dioxide concentration over terrestrial ecosystems as derived from eddy covariance measurements, *Atmos. Environ.*, *114*, 75–82, doi:10.1016/j.atmosenv.2015.05.026.

Luftmessnetz des Umweltbundesamtes (2015), WMO World Data Centre for Greenhouse Gases, Germany. [Available at http://ds.data.jma.go.jp/gmd/wdcgg/cgi-bin/wdcgg/download.cgi?index=SSL647N00-UBAG&param=200612120147&select=parameter&parac=observation.]

Marcotullio, P. J., A. Sarzynski, J. Albrecht, N. Schulz, and J. Garcia (2013), The geography of global urban greenhouse gas emissions: An exploratory analysis, *Clim. Change*, *121*(4), 621–634, doi:10.1007/s10584-013-0977-z.

Moffat, A. M., et al. (2007), Comprehensive comparison of gap-filling techniques for eddy covariance net carbon fluxes, *Agric. For. Meteorol.*, *147*(3–4), 209–232, doi:10.1016/j.agrformet.2007.08.011.

Moncrieff, J., R. Clement, J. Finnigan, and T. Meyers (2005), Averaging, detrending, and filtering of Eddy covariance time series, in *Handbook of Micrometeorology*, vol. 29, pp. 7–31, Kluwer Acad., New York, doi:10.1007/1-4020-2265-4_2.

Moncrieff, J. B., J. M. Massheder, H. de Bruin, J. Elbers, T. Friborg, B. Heusinkveld, P. Kabat, S. Scott, H. Soegaard, and A. Verhoef (1997), A system to measure surface fluxes of momentum, sensible heat, water vapour and carbon dioxide, *J. Hydrol.*, *188–189*, 589–611, doi:10.1016/s0022-1694(96)03194-0.

Moriwaki, R., and M. Kanda (2004), Seasonal and diurnal fluxes of radiation, heat, water vapor, and carbon dioxide over a suburban area, *J. Appl. Meteorol.*, *43*(11), 1700–1710, doi:10.1175/jam2153.1.

Park, M.-S., S. J. Joo, and S.-U. Park (2014), Carbon dioxide concentration and flux in an urban residential area in Seoul, Korea, *Adv. Atmos. Sci.*, *31*(5), 1101–1112, doi:10.1007/s00376-013-3168-y.

Pataki, D. E., P. C. Emmi, C. B. Forster, J. I. Mills, E. R. Pardyjak, T. R. Peterson, J. D. Thompson, and E. Dudley-Murphy (2009), An integrated approach to improving fossil fuel emissions scenarios with urban ecosystem studies, *Ecol. Complexity*, *6*(1), 1–14, doi:10.1016/j.ecocom.2008.09.003.

Pawlak, W., K. Fortuniak, and M. Siedlecki (2011), Carbon dioxide flux in the centre of Łódź, Poland-analysis of a 2-year eddy covariance measurement data set, *Int. J. Climatol.*, *31*(2), 232–243, doi:10.1002/joc.2247.

Ramamurthy, P., and E. R. Pardyjak (2011), Toward understanding the behavior of carbon dioxide and surface energy fluxes in the urbanized semi-arid Salt Lake Valley, Utah, USA, *Atmos. Environ.*, *45*(1), 73–84, doi:10.1016/j.atmosenv.2010.09.049.

Raupach, M. R., and R. H. Shaw (1982), Averaging procedures for flow within vegetation canopies, *Boundary Layer Meteorol.*, *22*(1), 79–90, doi:10.1007/bf00128057.

Reichstein, M., et al. (2005), On the separation of net ecosystem exchange into assimilation and ecosystem respiration: Review and improved algorithm, *Global Change Biol.*, *11*(9), 1424–1439, doi:10.1111/j.1365-2486.2005.001002.x.

Reid, K. H., and D. G. Steyn (1997), Diurnal variations of boundary-layer carbon dioxide in a coastal city—Observations and comparison with model results, *Atmos. Environ.*, *31*(18), 3101–3114, doi:10.1016/s1352-2310(97)00050-2.

Rosenzweig, C., W. Solecki, S. A. Hammer, and S. Mehrotra (2010), Cities lead the way in climate-change action, *Nature*, *467*(7318), 909–911, doi:10.1038/467909a.

Rotach, M. (1995), Profiles of turbulence statistics in and above an urban street canyon, *Atmos. Environ.*, *29*(13), 1473–1486, doi:10.1016/1352-2310(95)00084-c.

Rotach, M. W. (1993), Turbulence close to a rough urban surface part I: Reynolds stress, *Boundary Layer Meteorol.*, *65*(1–2), 1–28, doi:10.1007/bf00708816.

Schmidt, A., T. Wrzesinsky, and O. Klemm (2008), Gap filling and quality assessment of CO_2 and water vapour fluxes above an urban area with radial basis function neural networks, *Boundary Layer Meteorol.*, *126*(3), 389–413, doi:10.1007/s10546-007-9249-7.

Song, T., and Y. Wang (2012), Carbon dioxide fluxes from an urban area in Beijing, *Atmos. Res.*, *106*, 139–149, doi:10.1016/j.atmosres.2011.12.001.

Statistisches Amt Basel-Stadt (2015), Präsidialdepartement, Switzerland. [Available at http://www.statistik-bs.ch/tabellen.]

Strong, C., C. Stwertka, D. R. Bowling, B. B. Stephens, and J. R. Ehleringer (2011), Urban carbon dioxide cycles within the Salt Lake Valley: A multiple-box model validated by observations, *J. Geophys. Res.*, *116*, D15307, doi:10.1029/2011JD015693.

Tans, P., and R. Keeling (2015), NOAA/ESRL, Scripps Inst. of Oceanogr. [Available at scrippsco2.ucsd.edu/.]

University of Bern (2015), WMO World Data Centre for Greenhouse Gases, Switzerland. [Availalbe at http://ds.data.jma.go.jp/gmd/wdcgg/cgi-bin/wdcgg/download.cgi?index=JFJ646N00-KUP&param=201106030001&select=inventory.]

Valentino, F. L., M. Leuenberger, C. Uglietti, and P. Sturm (2008), Measurements and trend analysis of O_2, CO_2 and delta13C of CO_2 from the high altitude research station Junfgraujoch, Switzerland--A comparison with the observations from the remote site Puy de Dome, France, *Sci. Total Environ.*, *391*(2–3), 203–210, doi:10.1016/j.scitotenv.2007.10.009.

Velasco, E., S. Pressley, E. Allwine, H. Westberg, and B. Lamb (2005), Measurements of CO_2 fluxes from the Mexico City urban landscape, *Atmos. Environ.*, *39*(38), 7433–7446, doi:10.1016/j.atmosenv.2005.08.038.

Velasco, E., M. Roth, S. H. Tan, M. Quak, S. D. A. Nabarro, and L. Norford (2013), The role of vegetation in the CO_2 flux from a tropical urban neighbourhood, *Atmos. Chem. Phys.*, *13*(20), 10,185–10,202, doi:10.5194/acp-13-10185-2013.

Velasco, E., R. Perrusquia, E. Jiménez, F. Hernández, P. Camacho, S. Rodríguez, A. Retama, and L. T. Molina (2014), Sources and sinks of carbon dioxide in a neighborhood of Mexico City, *Atmos. Environ.*, *97*, 226–238, doi:10.1016/j.atmosenv.2014.08.018.

Vickers, D., and L. Mahrt (1997), Quality control and flux sampling problems for tower and aircraft data, *J. Atmos. Oceanic Technol.*, *14*(3), 512–526, doi:10.1175/1520-0426(1997)014<0512:qcafsp>2.0.co;2.

Vogt, R. (1995), Theorie, Technik und Analyse der experimentellen Flussbestimmung am Beispiel des Hartheimer Kieferwaldes: Ein Beitrag zu den Energiebilanzuntersuchungen im Reklip, *Stratus*, *3*, 1–101.

Vogt, R., A. Christen, M. W. Rotach, M. Roth, and A. N. V. Satyanarayana (2005), Temporal dynamics of CO_2 fluxes and profiles over a Central European city, *Theor. Appl. Climatol.*, *84*(1–3), 117–126, doi:10.1007/s00704-005-0149-9.

Webb, E. K., G. I. Pearman, and R. Leuning (1980), Correction of flux measurements for density effects due to heat and water vapour transfer, *Q. J. R. Meteorol. Soc.*, *106*(447), 85–100, doi:10.1002/qj.49710644707.